HHS Public Access

Author manuscript

J Immunol. Author manuscript; available in PMC 2017 February 01.

Published in final edited form as:

J Immunol. 2016 February 1; 196(3): 1013–1025. doi:10.4049/jimmunol.1501570.

Tertiary lymphoid tissue forms in retinas of mice with spontaneous autoimmune uveitis and has consequences on visual function

Jennifer L. Kielczewski[*], **Reiko Horai**[*], **Yingyos Jittayasothorn**[*], **Chi-Chao Chan**[*], and **Rachel R. Caspi**[*,‡]

[*]Laboratory of Immunology, National Eye Institute, National Institutes of Health, Bethesda, MD 20892-1857, USA

Abstract

During chronic inflammation, tertiary lymphoid tissue (TLT) can form within an inflamed organ, including the central nervous system (CNS). However, little is known about TLT formation in the neuroretina. In a novel spontaneous autoimmune mouse model of uveitis (R161H), we identified well-organized lymphoid aggregates in the retina and examined them for TLT characteristics. Presence of immune cells, tissue-specific markers, and gene expression patterns typically associated with germinal centers and T follicular helper (T_{FH}) cells were examined using immunohistochemistry and gene analysis of laser capture microdissected retina. Our data revealed the retinal lymphoid structures contained $CD4^+$ T cells and B cells in well-defined zonal areas that expressed classic germinal center markers, PNA and GL-7. Gene expression analysis showed upregulation of T follicular helper cell markers, most notably CXCR5 and its ligand CXCL13, and immunohistochemical analysis confirmed CXCR5 expression, typically associated with $CD4^+$ T follicular helper cells. Highly organized stromal cell networks, a hallmark of organized lymphoid tissue, were also present. Positive staining for phospho-Zap70 in retina-specific T cells indicated $CD4^+$ T cells were being activated within these lymphoid structures. $CD138^+/B220^+$ plasma cells were detected, suggesting the retinal lymphoid aggregates give rise to functional germinal centers, which produce antibodies. Interestingly, eyes with lymphoid aggregates exhibited lower inflammatory scores by fundus examination and a slower initial rate of loss of visual function by electroretinography, compared to eyes without these structures. Our findings suggest that the lymphoid aggregates in the retina of R161H mice represent organized TLT, which impact the course of chronic uveitis.

Keywords

autoimmune disease; uveitis; retina; inflammation; tertiary lymphoid tissue; germinal center

[‡]Corresponding Author. 10 Center Drive 10N222 Bethesda, MD 20892 Tel.: +301 435 4555 Fax: +301 480 6668 caspir@mail.nih.gov or caspi@helix.nih.gov (R.R. Caspi).

Disclosures: None declared

INTRODUCTION

Ectopic or tertiary lymphoid tissues (TLT) develop at sites of inflammation or infection in peripheral, non-lymphoid organs. These tissues are structurally similar to secondary lymphoid organs with distinct B and T cell compartmentalized areas that contain germinal center formations comprised of T follicular helper cells (T_{FH}), which provide help to B cells for the generation of long-lived plasma cells or antibodies (1). Germinal centers require T_{FH} cells for their formation and maintenance and are responsible for providing protective humoral or immunological memory. TLT has been associated with local pathology in a number of diseases resulting from chronic infection, inflammation, or autoimmunity (2–4). For example, TLT has been reported in the joints of patients with rheumatoid arthritis, (5) salivary glands in Sjögren's syndrome, (6–8) the thyroid in Grave's disease, (9) the pancreas in diabetes, (10, 11) the central nervous system in multiple sclerosis, (1, 12, 13) and the choroid in the late stage of sympathetic ophthalmia (14). In many cases, formation of well-developed TLT correlates with increased severity of disease and local production of autoantibodies (2, 4). However, there are also reports in which TLT can contribute to protective immune responses, such as in viral infections, to promote an antiviral response (15) and in certain cancers (16–18).

In patients, lymphoid aggregates have been reported to form in ocular tissues, despite the immune privileged status of the eye. However, it is not always clear whether these structures can be considered true "lymphoid tissue" due to the fact that they were reported under malignant or benign neoplastic conditions and there is no data supporting that they express characteristic lymphoid tissue markers. Lymphoid-like tissue in the uvea has been described as reactive lymphoid hyperplasia or intraocular pseudotumor with benign inflammatory disease (19). Patients with this diagnosis were reported to have long-lasting inflammatory cell infiltrate, including plasma cells, lymphocytes, and macrophages. Lymphoid follicle formation, based on histological criteria, has been reported in spontaneous, as well as, in experimentally induced uveitis in horses (20, 21). However, no immunological characterization was performed. Definitive identification and characterization of lymphoid tissue in the human eye is complicated by the fact that chronically inflamed human ocular tissues are limited and not readily available for these types of studies.

Recently, a spontaneous autoimmune mouse model of uveitis in R161H TCR transgenic mice was developed by Horai et al (22). These mice express a TCR specific for the retinal antigen interphotoreceptor retinoid-binding protein (IRBP) and develop spontaneous uveitis with 100% incidence by 8 weeks of age. The disease is characterized by retinal and choroidal inflammation, retinal vasculitis, photoreceptor destruction, and loss of visual function (22–24). Thus, this model reproduces many essential clinicopathological features of human uveitis, which is estimated to cause 10–15% of blindness in the Western world (25, 26).

Interestingly, approximately 40% of R161H mice develop well-organized retinal lymphoid aggregates with a distinct histology reminiscent of TLT. In this study, we thoroughly characterized the retinal lymphoid aggregates using laser capture microdissection and immunohistochemistry with respect to the defining TLT attributes, namely, presence of

distinct cellular markers for B&T cell segregation, presence of high endothelial venules (HEVs) and development of follicular dendritic cell (FDC) networks that support germinal center responses, such as formation of T_{FH} cells. Multi-color immunohistochemical staining was chosen in preference to flow cytometry to *(i)* preserve the spatial organization of the localized TLT, *(ii)* to facilitate visualization of cellular expression patterns within the TLT and *(iii)* to exclude infiltrating cells that are present outside the aggregates, which would confound interpretation of the TLT if analyzed by flow cytometry. Our findings lead to the conclusion that the retinal lymphoid aggregates in R161H mouse retinas represent TLT with organized germinal centers that contain B cells and T follicular helper cells within an extensive stromal cell network and show evidence of immune cell signaling, activation, and plasma cell formation. Unexpectedly, while presence of immunologically active lymphoid structures would likely contribute to disease progression, clinical scores, as well as, retinal function of mice with TLT indicated the opposite. Retinas of mice with aggregates showed less active inflammation and a slower deterioration of visual function than retinas of mice without these structures. It remains to be established whether formation of TLT within the retina is the result of a slower and more chronic disease process, or its cause.

MATERIALS AND METHODS

Animals

IRBP TCR transgenic R161H mice on the B10.RIII background, described by Horai et al. (22) aged 8–16 weeks were used in all experiments. Age matched wild-type (WT) B10.RIII were used as controls. Animal care and use were in complete compliance with the guidelines of the National Institutes of Health and with the ARVO statement for the Use of Animals in Ophthalmic and Vision Research.

Antibodies

The following antibodies were used for confocal microscopy at 1:25–1:100 concentrations. Primary antibodies to anti-CD4-alexa fluor 660 conjugated, anti-B220-FITC conjugated, anti-CD8, biotin labeled-PNA, anti-GL-7, biotin labeled-anti IgD, anti-Ki-67, anti-Bcl-6, anti-CD80, and anti-Gata-3 were all purchased from eBioscience (San Diego, CA). Anti-CD11c-FITC and anti-PNAd was purchased from BioLegend (San Diego, CA). Anti-CXCR5, anti-MHC II (IA/IE), anti-FDC-1, anti-CD138, anti-MAdCAM-1, and anti-CD35 were all purchased from BD Biosciences (San Diego, CA). Anti-F4/80 was purchased from AbD Serotec, (Raleigh, NC) anti-phosph-Zap70 was obtained from Cell Signaling Technologies (Beverly, MA) and anti-Iba-1 was acquired from Wako Chemicals USA (Richmond, VA). Both anti-CD3 and anti-CXCL13 were obtained from R&D (Minneapolis, MN). The IRBP p161-180/MHCII/IgG dimer reagent was made in our lab (27) and is not commercially available.

Clinical Evaluation and Scoring of Uveitis

For clinical examinations (funduscopy) and experimental procedures (ERG, fluorescein angiography) systemic anesthesia was administered by intraperitoneal injection with a ketamine/xylazine mixture (77mg/kg+4.6mg/kg respectively). Local ocular surface anesthesia was applied (0.5% Alcaine drops). The pupils were dilated with 0.5%

Tropicamide and 0.5% phenylephrine hydrochloride. All mice were examined for clinical signs of uveitis using a binocular fundus microscope with coaxial illumination. Mice with distinct retinal aggregates were identified. These lesions are generally bright, circular white aggregates, with a well-defined structure seen under the microscope. Clinical uveitis was scored on a scale of 0 (no disease) to 4 (maximum disease) in half point increments based on the number of retinal lesions and severity of inflammation as previously described (24).

Histology

Eyes were harvested and fixed in 4% paraformaldehyde, cryo-embedded in Optimum Cutting Temperature (OCT) Tissue-Tek media (Fisher Scientific) with 20% sucrose, and sectioned at 10 microns through the optic nerve plane using a cryostat (Leica Microsystems, Mannheim, Germany). The tissue sections were stained with hematoxylin-eosin (H&E) and imaged using a Zeiss Imager microscope (Carl Zeiss, Munich, Germany).

Immunohistochemistry

Eyes were collected and cryopreserved in 2:1 OCT with 20% sucrose. The tissue blocks were stored at −80 degrees until cutting into 10 micron sections onto slides that were stored at −80 degrees until use. Frozen retinal sections were allowed to defrost at room temperature and were then fixed in acetone for 10 minutes followed by blocking with 10% normal goat serum at room temperature for 1 hour. The tissue was washed with PBS for 10 minutes. Primary antibodies were applied at 1:25–1:100 dilution for 1–2 hours at room temperature or overnight at 4°C in humid chambers to prevent the slides from drying out. The sections were then washed with PBS three times for 10 minutes. If the primary antibody was not directly conjugated to a fluorochrome then an Alexa Fluor-568, 594, or 488 secondary or a streptavidin 568 or 488-labeled secondary antibody (Life Technologies, Grand Island, NY) was applied at 1:500 for 1 hour at room temperature. The slides were then washed three times in PBS and mounted with Vectashield containing DAPI (Vector Labs, Burlingame, CA).

Confocal Microscopy and Imaging

Retinas were imaged using a Zeiss confocal laser-scanning microscope (LSM700 or LSM780). Images were processed for brightness and contrast using ImageJ software (http://rsb.info.nih.gov/ij/) or Adobe Photoshop (Adobe systems, San Jose, CA). Confocal microscopy was performed with set parameters for laser power, photomultiplier gain, and offset, with a pinhole of diameter of 1 Airey unit. Brightest point projections of z-stacks (5–10 optical sections, 0.5–1 mm thickness, 0.5–1 mm step size) were acquired.

Laser Capture Microdissection (LCM)

Whole mouse globes were embedded and frozen in OCT compound (BioTek) immediately following enucleation and stored at −80 degrees overnight. The blocks were cut into 20μm sections and collected on polyethylene naphthalate RNase free glass slides (Carl Zeiss, Munich, Germany). Sections were dehydrated with 70%, 95% and 100% ethanol and xylene for 15 seconds each using RNase free reagents, followed by staining with Cresyl violet for 30 seconds. After the sections were air dried for 10 minutes, the retinal aggregates were

microdissected using a Zeiss Palm LCM. The retinal aggregates were easily identified by their distinctive morphologic appearance in the stained retinal tissue sections. Approximately 20–30 retinal lesions were collected to maximize RNA yield. Microdissected tissue was directly collected into LCM capture caps containing lysis buffer from the PicoPure RNA isolation kit (Invitrogen, Eugene, OR). Typical laser settings were 7.5μm spot for diameter, 0.7–1.2 ms for duration, and 60–80 mW for laser power.

RNA isolation

RNA from a total of five mice from each group was pooled together in three independent experiments. RNA was extracted from microdissected tissue with a PicoPure RNA isolation kit following the manufacturer's suggested protocol. All RNA samples were linearly amplified with an amplification kit (Invitrogen, Eugene, OR). For LCM, two rounds of amplification were needed to provide adequate material for analysis using an AMP kit (Invitrogen, Eugene, OR). The integrity of the RNA was assessed using a bioanalyzer (model 2100: Agilent technologies, Palo Alto, CA) or using a Nanodrop (Fisher Scientific, Grand Island, NY).

RT-PCR

Isolated mRNA was converted to cDNA using manufacturer's protocol (Invitrogen). PCR amplification was carried out using a Customized 48 Format Taqman plate (Life Technologies, Grand Island, NY) on an Applied BioSystems 7500 Fast real-time PCR system with ABI primers (Life Technologies, Grand Island, NY). Data were analyzed by Comparative CT (DDCT) method using ABI 7500 software v2.0.6 software (Life Technologies, Grand Island, NY). All samples were normalized to GAPDH. Gene expression in laser captured R161H retinal aggregates was compared to adjacent R161H retina without lymphoid aggregates. The positive control was true lymphoid follicles, isolated from immunized lymph nodes of EAU mice 7 days after immunization.

ELISA

Autoantibodies against the retinal antigen IRBP in mouse serum was analyzed by ELISA. Briefly, 96-well ELISA plates were coated overnight with IRBP 161-180 peptide (100 μL of 5 μg/mL) in 0.1 M $NaHCO_3$ (pH 8.2). The plates were rinsed with washing buffer (PBS pH 7.5, with 0.5% Tween 20) and were blocked with blocking buffer (PBS-Tween with 0.1% BSA) for 2 hours at room temperature. After two washes, serially diluted serum samples were added to the wells in triplicate, and the plates were incubated overnight at 4°C. After 4 washes, biotinylated anti-mouse IgG was applied for 1 hour, followed by 4 washes. Streptavidin-HRP conjugate (1:5000) was added to the plate for 30 minutes at 37°C, followed by 4 washes. Color reaction was performed with TMB (Thermo Scientific, Rockford, IL) substrate and was terminated by addition of 2N H_2SO_4. The plates were read at 450 nm with an ELISA reader (Molecular Devices, Sunnyvale CA).

Fluorescein Angiography

Mice were anesthetized with ketamine/xylazine. Pupils were dilated using 1% Tropicamide and 2.5% phenylephrine. 50μl of fluorescein was injected through the tail vein and

angiographic images were captured using a Micron III system (Phoenix Research Labs, Inc. Pleasanton, CA). Initial images were taken immediately after fluorescein injection and then 1 minute later to show vascular leakage accumulation.

Electroretinography (ERG)

Retinal function was evaluated by recording of dark-and light-adapted ERG with the Espion E2 System (Diagnosys LLC, Lowell, MA). Mice were dark adapted overnight and all procedures were performed under dim red light. Only mice in which the ocular media was clear (absent of cataract or corneal opacity) as determined by fundus examination were subjected to ERG analysis. The mouse eyes were carefully examined to ensure they were clear and free of vitreous infiltrates so as not to interfere with the accuracy of the ERG recordings. All of the mice were anesthetized and their pupils dilated as described above. For the ERG recordings, electrodes were placed on the center of the cornea. Reference and ground electrodes were attached to the mouth and placed subcutaneously in the posterior neck-back region respectively. The a-wave amplitude was measured from the baseline to the trough of the a-wave and b-wave amplitude was measured from the trough of the a-wave to the peak of the b-wave.

Statistical Analysis

All data are expressed as the mean ± SEM. For comparison of two groups, *P* values were determined by the unpaired two-tailed Student's *t*-test and paired data were analyzed by the paired Student's *t*-test. For comparison of more than two groups, significant values were calculated via one-way or two-way ANOVA to reveal differences in the data sets followed by Dunn's or Tukey's Multiple comparison *post-hoc* test. Statistical analyses were performed using GraphPad Prism 6 software. Probability values of $p \leq 0.05$ were considered statistically significant.

RESULTS

Mice with spontaneous uveitis progressively develop retinal lymphoid aggregates in the neuroretina

The retina is normally a neuronal structure with a well-organized architecture (Fig. 1 A–B and Fig. 2 A–C) but inflammation can lead to loss of retinal morphology and structure. In eyes of spontaneously uveitic R161H mice, two distinct types of disease were observed. One type consisted of diffuse retinal damage accompanied by widespread loss of retinal morphology (Fig. 1 C–D). This type of disease resembled the pathology often seen in experimental autoimmune uveoretinitis (EAU) (28) induced by active immunization of WT mice with IRBP in complete Freund's adjuvant (CFA) (29). A second type was characterized by development of growing retinal lymphoid aggregates that are not seen in EAU, with relative preservation of retinal architecture outside of the lymphoid aggregate structures (Fig. 1 E–H).

Upon closer examination, these aggregates bear a strong resemblance histologically to secondary lymphoid structures that can be seen in spleen and lymph nodes and to tertiary lymphoid structures that can form in chronically inflamed tissues (12). Repeated

fundoscopic examinations revealed that these retinal lymphoid aggregates begin as small, round lesions and typically increase in size, around 7–10 weeks of age, growing progressively, to occupy large portions of the retina and even choroid (Fig. 1 E–H and Fig. 2 G, J). Using the scoring system developed for EAU, which quantitates the disease based on intensity of inflammation, as well as the number, size and type of lesions, (26, 29) eyes containing lymphoid aggregates possessed statistically lower clinical and histological disease scores compared with age-matched mice lacking these defined lymphoid structures (Fig. 1 I, J).

The retinal lymphoid aggregates appear as distinct, bright white circular lesions with sharply defined borders in the fundus of R161H mice (Fig. 2 G, J). In contrast, eyes lacking these lesions display diffuse inflammation throughout the retina as depicted in Fig. 2 D–F. While the blood retinal barrier (BRB) integrity around the retinal lymphoid aggregates as shown by leakage of fluorescein from the retinal vessels is disrupted (Fig. 2 H–I and K–L), the overall leakage pattern in eyes with aggregates appears more focal, with less widespread disruption to the BRB compared to eyes without retinal aggregates (Fig. 2 E–F).

Diverse immune cell types, including IRBP specific T cells, are present in retinal lymphoid aggregates

Immunohistochemical staining revealed that the retinal aggregates are composed predominately of $B220^+$ B cells and $CD4^+$ T cells. We counted immuno-labeled cells in well-defined retinal lymphoid aggregates and found that approximately 30% of the retinal lymphoid aggregates were made up of $CD4^+$ T cells, while 60% were $B220^+$ B cells. Approximately 10% were $CD8^+$ T cells (Fig. 3 A–J). Both B cells and $CD4^+$ T cells show evidence of proliferation by co-staining with Ki-67, a cell proliferation marker (Fig. 3 K–O). The retinal lymphoid aggregates also contain R161H $TCR^+/CD4^+$ IRBP-specific T cells, as revealed by immunohistochemical staining with a specific IRBP161-180-MHC-class II dimer, (30) which detects cells bearing an IRBP-specific TCR (Fig. 3 P–T). We also detected macrophages and microglia (Supplemental Fig. 1), both of which are able to act as antigen presenting cells, (26, 31–33) as well as $FoxP3^+/CD4^+$ T cells, which are likely to represent regulatory T cells (Supplemental Fig. 2). On average, approximately 25% of the $CD4^+$ T cells in the retinal aggregates were $CD4^+/FoxP3^+$ as determined by counting immuno-labeled retinal cross-sections containing distinct retinal lymphoid aggregates.

Retinal lymphoid aggregates express germinal center markers and T_{FH} associated genes, consistent with tertiary lymphoid tissue

By immunohistochemistry, the retinal lymphoid aggregates stain positively for the classical germinal center markers PNA and GL-7 (11, 26) (Fig. 4 A–H). They also contain $GL\text{-}7^+/B220^+$ cells, which are typically found in germinal centers (26) (Fig. 4 I–L). Furthermore, they have low expression of IgD, which is characteristic of germinal centers in secondary lymphoid tissue (26, 34) (Fig. 4 M–P). In order to study whether characteristic T_{FH} genes are upregulated, we isolated the retinal lymphoid aggregates by laser capture microdissection. Gene array expression profiling revealed that retinal lymphoid aggregates express elevated T_{FH} genes including Gata-3, Bcl-6, and IL-6, in a pattern similar to lymph node tissue from WT mice that had been immunized for EAU with the retinal antigen IRBP

(Fig. 5 A). Immunohistochemical staining confirmed high expression of Gata-3 and Bcl-6 at the protein level in the retinal aggregates (Fig. 5 B–C), both of which are important transcriptional regulators in driving T_{FH} cell differentiation. Similarly, CXCR5, which is a chemokine receptor expressed by T_{FH} cells, (35) as well as its ligand CXCL13 (Fig. 5 A and Fig. 6 K–O), was statistically higher in R161H retinas with the retinal aggregates compared to retinas of R161H mice without these structures. $CXCR5^+/CD4^+$ T cells were detectable within the retinal aggregates (Fig. 6 A–J). These data support the notion that the retinal lymphoid aggregates represent bona fide tertiary lymphoid tissue.

Retinal lymphoid aggregates contain extensive high endothelial venules and structural networks that can support immune cell signaling and activation

Organized lymphoid follicles typically contain high endothelial venules (HEVs). These specialized post-capillary venous swellings are important in lymphocyte recruitment and trafficking. HEVs typically have characteristic “plump” appearance. Characteristic markers for HEVs include MAdCAM-1 (MECA-367) and PNAd (MECA-79). Both of these markers were especially prominent in large retinal lymphoid aggregates (Fig. 7 F–O). In addition, we also detected Lyve-1-positive lymphatic vessels (Fig. 7 A–E). The retinal aggregates also contained extensive stromal and follicular dendritic cells networks (FDCs) (Fig. 8). These structural elements are known to be essential for lymphoid tissue formation, organization and function, and were particularly prominent in well developed retinal aggregates containing a large number of B cells.

Since the retinal aggregates contain well-organized stromal and dendritic cell networks, we hypothesized that they might support immune cell signaling and activation. Fig. 9 shows the presence of IRBP-specific $CD4^+$ T cells in close association with $CD11c^+$ cells, a marker characteristic of professional antigen-presenting dendritic cells (Fig. 9 A–L). Positive staining for phospho-Zap70 in these cells indicates that their TCR received a signal. We also show that $CD4^+$ T cells are closely associated with $CD11c^+$ cells co-localized with CD80, which is a co-stimulatory molecule needed for T cell activation (Fig. 9 M–R). Together, these results suggest that endogenous IRBP is presented by $CD11c^+$ dendritic cells to activated $CD4^+$ T cells in the retinal TLT structures (Fig. 9).

Plasma cells are present in the retinal lymphoid aggregates

Since there is evidence of T cell signaling and activation in the retinal TLT, we examined generation of plasma cells and retina-specific auto-antibodies. By immunohistochemical staining, $CD138^+/B220^+$ cells were found localized within the retinal aggregates (Fig. 10 A–J). Interestingly, large well-developed retinal TLT were where $CD138^+$ cells were typically found. This in in line with the observation that stromal cell networks are highly organized within the large retinal aggregates, which may support immune cell signaling and promote inflammatory cell responses. It is within the late-stage retinal TLT, where plasma cells are most frequently seen and generated. We next examined the serum of mice with large retinal TLT structures for the presence of IRBP-specific auto-antibodies (Fig. 10 K). Interestingly, mice with retinal TLT had higher serum antibodies against IRBP compared to mice without retinal TLT. It is unknown, however, how much of the serum antibody in fact originated in

the retina and diffused into the serum through the disrupted BRB, or how much may have leaked out of the eye into the draining lymph nodes.

Eyes with TLT initially retain better visual activity than eyes with diffuse disease, but progressive growth of the TLT is associated with visual decline

Our previous study demonstrated that mice with uveitis, whether induced by immunization or spontaneous onset, progressively lose visual function (23). In order to determine whether the retinal TLT contributes to loss of visual function, we tested visual activity using electroretinography in young mice (7–10 weeks old) with early TLT and in older mice (11–12 week old) with large, late-stage TLT structures, compared to age-matched R161H mice with uveitis, whose eyes were completely devoid of retinal TLT and healthy wild type controls (Fig. 11). Notably, in mice that displayed similar clinical disease scores, eyes containing retinal TLT were initially associated with better retention of visual function compared to inflamed R161H eyes lacking retinal TLT, as evidenced by a statistically higher light b wave and dark a wave ERG response (Fig. 11 B–C). However, as the TLT becomes increasingly spread out with age and losing its focal organization, this advantage was lost and visual function in 10–11 week old mice with late-stage TLT was similar to R161H mice devoid of retinal TLT (Fig. 11). The mice with late-stage diffuse infiltrates are more pathogenic on visual activity than the early-stage focal infiltrates, in part due to their disintegration. The late-stage TLT is made up of more disorganized follicles and/or infiltrates, which can spread throughout the retina and replace extensive areas of healthy retinal tissue, similar to what occurs in R161H mice lacking non-retinal TLT.

DISCUSSION

The mouse model of experimental autoimmune uveitis, or EAU, induced in B10.RIII mice by immunization with the retinal protein IRBP or its major pathogenic peptide IRBP161-180, has been developed some time ago and its pathology is well characterized. Typically, EAU in B10.RIII mice is acute and involves destruction of retinal tissues with widespread inflammatory infiltrates. Interestingly, in the recently developed spontaneous uveitis model in R161H mice, also on the B10.RIII background, approximately 40% of mice develop distinct retinal lymphoid aggregates. These aggregates start as small lesions around 2 months of age (about a month after clinical disease onset) and with time grow and coalesce into large lymphoid structures that can also involve the choroid. Tertiary lymphoid structures have been reported in many other chronically inflamed tissues, including the brain and eye. However, to our knowledge, this is the first comprehensive study, histologically and functionally, of TLT and its impact on visual function in a spontaneous model of autoimmune uveitis. The retinal lymphoid aggregates are organized structures that appear to function as true lymphoid follicles and support cellular interactions, whereas the typical widespread inflammatory infiltrates seen in EAU models appear to be composed of disorganized or diffuse cell infiltrates, which do not support a cellular niche like that of the TLT we describe here.

Extensive analysis of cellular markers and expressed genes revealed that the retinal lymphoid aggregates fit the criteria of organized TLT. Specifically, we show they have a

germinal center phenotype that is $PNA^+/GL\text{-}7^+/IgD^{lo}$. The retinal TLT contain distinct B and T cell zones along with microglia and macrophages. Macrophages are typically found in secondary lymphoid tissue and microglial cells share many characteristics similar to that of macrophages (26, 36). The retinal TLT structures contain elevated T follicular helper genes. We also detected presence of T_{FH} cells immunohistochemically that are $CXCR5^+/CD4^+$ and are localized directly within the retinal TLT. The retinal TLT tissue contains extensive stromal cell and follicular dendritic cells networks, which are important in secondary lymphoid tissue. These networks support migration of cells and inflammatory cell responses, such as formation of antibodies in lymphoid tissue. The retinal TLT, thus, possesses the cellular attributes of a dynamic structure that facilitates cell proliferation and activation of immune cells.

It is interesting that only 40% of R161H mice develop these TLT structures and further investigation is needed into what drives their formation in ocular tissues. It is an open question whether they represent a cause, or an effect, of the more chronic nature of R161H uveitis, compared to immunization-induced EAU. Also, of interest would be to explore their dependence on Th17 *vs*. Th1 cytokines. In the lung and brain, IL-17 was reported to play a critical role in TLT formation, (37, 38) but in the stomach Th1 dependent formation of follicles was reported (39). In contrast to these previous reports, we did not detect upregulation of IL-17 in the retinal TLT of R161H mice. The chemokine CXCL13 is important in cytokine production by effector T cells, and CXCL13 expression was clearly detectable in the retinal TLT as shown in Fig. 6. However, we did not detect upregulation of other chemokines, such as CCL19 or CCL21, which also orchestrate cell migration in lymphoid tissue.

We believe that formation of these structures is driven at least in part by chronic antigenic stimulation within the retina. Previous studies from others, demonstrated at the functional level, that retinal antigen presentation and retina-specific T cell activation, and even priming of previously naïve T cells does occur in the living eye (40–43). In fact, numerous studies indicate that antigen recognition within the retina by infiltrating uveitogenic T cells is a prerequisite for initiation of the inflammatory cascade and induction of uveitis (40–42, 44). An important finding of this work is, therefore, the demonstration that immune signaling in fact occurs in the retina within the retinal TLT, as evidenced by phosphorylation of Zap70 in IRBP-specific T cells found in close association with $CD11c^+$ (antigen-presenting) cells. Our data do not reveal whether these are naïve IRBP specific T cells encountering antigen for the first time, or whether these are T cells previously primed in the periphery on environmental cross-reactive antigens that are re-encountering their antigen within the retina (45).

Irrespective of whether these are naïve or memory T cells, the TLT in the retina can serve as a source of antigen specific T cells, which can be activated (or re-activated) and proliferate in these structures, as evidenced by co-staining for Ki67. Alternatively, the retinal aggregates might serve to localize and sequester the antigen-specific T cells in the retina, potentially providing an explanation as to why eyes containing the retinal aggregates initially have a lower disease score and slower deterioration of visual function than eyes devoid of these structures. However, as these aggregates grow and develop over time and

show evidence of plasma cell accumulation, they can become a significant source of autoantibody production. Our earlier data showed that antibodies contribute to the severity of EAU (46) and there is evidence that in human uveitis, B cells may also play a pathogenic role (47–49). It is therefore tempting to speculate that this could be one of the factors that contribute to a higher level of serum antibodies and to increased loss of visual function in mice with well-developed TLT in the eye. Notably, even though we detected regulatory T cells within the TLT, it is unclear to what extent these T cells are functional and whether they, at least initially, limit disease severity. This question warrants further exploration.

Taken together, our data suggest that the retinal lymphoid aggregates in R161H retina are functional TLT structures which allow T cells, B cells and antigen presenting cells to interact in a highly organized manner on a matrix made up of stromal cells and are a local source for immune cell activation. Although lymphoid-like infiltration in human eyes with chronic uveitis have been reported, (19, 50) it is not clear at this point whether this represents true TLT, as inflamed retinal tissue cannot be easily obtained from patients for extensive analysis, such as was performed in this study. Our data point to the possibility that immunologically active TLT can form in the eye, which can have implications on clinical aspects of the disease. Our transgenic mouse model (R161H) allows greater study of retinal tertiary lymphoid tissue manifestation under chronic ocular inflammation and the potential mechanisms that drive its formation.

Supplementary Material

Refer to Web version on PubMed Central for supplementary material.

Acknowledgments

Grant Support: This work was supported through the NIH intramural research program in the National Eye Institute, Project# EY000184

The authors would like to thank the Histopathology Core facility (NEI) for H&E staining of histology slides and technical assistance. We would also like to thank the Vision Function Core Facility and the Biological Imaging Core Facility (NEI) for providing technical assistance with equipment.

Abbreviations

IRBP	Interphotoreceptor retinoid binding protein
TCR	T cell receptor
EAU	Experimental Autoimmune Uveitis
WT	wild type
TLT	tertiary lymphoid tissue
T_{FH}	T follicular helper cell
FDC	follicular dendritic cell
BRB	blood-retinal barrier
HEV	high endothelial venule

References

1. Neyt K, Perros F, GeurtsvanKessel CH, Hammad H, Lambrecht BN. Tertiary lymphoid organs in infection and autoimmunity. Trends in immunology. 2012; 33:297–305. [PubMed: 22622061]
2. Vinuesa CG, Sanz I, Cook MC. Dysregulation of germinal centres in autoimmune disease. Nature reviews Immunology. 2009; 9:845–857.
3. Vinuesa CG, Tangye SG, Moser B, Mackay CR. Follicular B helper T cells in antibody responses and autoimmunity. Nature reviews Immunology. 2005; 5:853–865.
4. Zhang X, Ing S, Fraser A, Chen M, Khan O, Zakem J, Davis W, Quinet R. Follicular helper T cells: new insights into mechanisms of autoimmune diseases. The Ochsner journal. 2013; 13:131–139. [PubMed: 23531878]
5. Takemura S, Klimiuk PA, Braun A, Goronzy JJ, Weyand CM. T cell activation in rheumatoid synovium is B cell dependent. Journal of immunology. 2001; 167:4710–4718.
6. Bombardieri M, Barone F, Lucchesi D, Nayar S, van den Berg WB, Proctor G, Buckley CD, Pitzalis C. Inducible tertiary lymphoid structures, autoimmunity, and exocrine dysfunction in a novel model of salivary gland inflammation in C57BL/6 mice. Journal of immunology. 2012; 189:3767–3776.
7. Stott DI, Hiepe F, Hummel M, Steinhauser G, Berek C. Antigen-driven clonal proliferation of B cells within the target tissue of an autoimmune disease. The salivary glands of patients with Sjogren's syndrome. The Journal of clinical investigation. 1998; 102:938–946. [PubMed: 9727062]
8. Reksten TR, Johnsen SJ, Jonsson MV, Omdal R, Brun JG, Theander E, Eriksson P, Wahren-Herlenius M, Jonsson R, Nordmark G. Genetic associations to germinal centre formation in primary Sjogren's syndrome. Annals of the rheumatic diseases. 2014; 73:1253–1258. [PubMed: 23606706]
9. Grogan JL, Ouyang W. A role for Th17 cells in the regulation of tertiary lymphoid follicles. European journal of immunology. 2012; 42:2255–2262. [PubMed: 22949324]
10. Kendall PL, Yu G, Woodward EJ, Thomas JW. Tertiary lymphoid structures in the pancreas promote selection of B lymphocytes in autoimmune diabetes. Journal of immunology. 2007; 178:5643–5651.
11. Luzina IG, Atamas SP, Storrer CE, daSilva LC, Kelsoe G, Papadimitriou JC, Handwerger BS. Spontaneous formation of germinal centers in autoimmune mice. Journal of leukocyte biology. 2001; 70:578–584. [PubMed: 11590194]
12. Carragher DM, Rangel-Moreno J, Randall TD. Ectopic lymphoid tissues and local immunity. Seminars in immunology. 2008; 20:26–42. [PubMed: 18243731]
13. Stuve O, Eagar TN. B cells, antibodies, and tertiary lymphoid tissue in MS brains. The Lancet Neurology. 2008; 7:766–767. [PubMed: 18702996]
14. Shah DN, Piacentini MA, Burnier MN, McLean IW, Nussenblatt RB, Chan CC. Inflammatory cellular kinetics in sympathetic ophthalmia a study of 29 traumatized (exciting) eyes. Ocular immunology and inflammation. 1993; 1:255–262. [PubMed: 22822781]
15. Lucchesi D, Bombardieri M. The role of viruses in autoreactive B cell activation within tertiary lymphoid structures in autoimmune diseases. Journal of leukocyte biology. 2013; 94:1191–1199. [PubMed: 23812327]
16. Di Caro G, Bergomas F, Grizzi F, Doni A, Bianchi P, Malesci A, Laghi L, Allavena P, Mantovani A, Marchesi F. Occurrence of tertiary lymphoid tissue is associated with T-cell infiltration and predicts better prognosis in early-stage colorectal cancers. Clinical cancer research: an official journal of the American Association for Cancer Research. 2014; 20:2147–2158. [PubMed: 24523438]
17. Pitzalis C, Jones GW, Bombardieri M, Jones SA. Ectopic lymphoid-like structures in infection, cancer and autoimmunity. Nature reviews Immunology. 2014; 14:447–462.
18. Wirsing AM, Rikardsen OG, Steigen SE, Uhlin-Hansen L, Hadler-Olsen E. Characterisation and prognostic value of tertiary lymphoid structures in oral squamous cell carcinoma. BMC clinical pathology. 2014; 14:38. [PubMed: 25177210]
19. Cheung MK, Martin DF, Chan CC, Callanan DG, Cowan CL, Nussenblatt RB. Diagnosis of reactive lymphoid hyperplasia by chorioretinal biopsy. American journal of ophthalmology. 1994; 118:457–462. [PubMed: 7943123]

20. Deeg CA, Ehrenhofer M, Thurau SR, Reese S, Wildner G, Kaspers B. Immunopathology of recurrent uveitis in spontaneously diseased horses. Experimental eye research. 2002; 75:127–133. [PubMed: 12137758]
21. Deeg CA, Thurau SR, Gerhards H, Ehrenhofer M, Wildner G, Kaspers B. Uveitis in horses induced by interphotoreceptor retinoid-binding protein is similar to the spontaneous disease. European journal of immunology. 2002; 32:2598–2606. [PubMed: 12207344]
22. Horai R, Silver PB, Chen J, Agarwal RK, Chong WP, Jittayasothorn Y, Mattapallil MJ, Nguyen S, Natarajan K, Villasmil R, Wang P, Karabekian Z, Lytton SD, Chan CC, Caspi RR. Breakdown of immune privilege and spontaneous autoimmunity in mice expressing a transgenic T cell receptor specific for a retinal autoantigen. Journal of autoimmunity. 2013; 44:21–33. [PubMed: 23810578]
23. Chen J, Qian H, Horai R, Chan CC, Caspi RR. Use of optical coherence tomography and electroretinography to evaluate retinal pathology in a mouse model of autoimmune uveitis. PloS one. 2013; 8:e63904. [PubMed: 23691112]
24. Chen J, Qian H, Horai R, Chan CC, Falick Y, Caspi RR. Comparative analysis of induced vs. spontaneous models of autoimmune uveitis targeting the interphotoreceptor retinoid binding protein. PloS one. 2013; 8:e72161. [PubMed: 24015215]
25. Gritz DC I, Wong G. Incidence and prevalence of uveitis in Northern California; the Northern California Epidemiology of Uveitis Study. Ophthalmology. 2004; 111:491–500. discussion 500. [PubMed: 15019324]
26. Rothova A, Suttorp-van Schulten MS, Frits Treffers W, Kijlstra A. Causes and frequency of blindness in patients with intraocular inflammatory disease. Br J Ophthalmol. 1996; 80:332–336. [PubMed: 8703885]
27. Karabekian Z, Lytton SD, Silver PB, Sergeev YV, Schneck JP, Caspi RR. Antigen/MHC class II/Ig dimers for study of uveitogenic T cells: IRBP p161–180 presented by both IA and IE molecules. Invest Ophthalmol Vis Sci. 2005; 46:3769–3776. [PubMed: 16186361]
28. Thaunat O, Graff-Dubois S, Brouard S, Gautreau C, Varthaman A, Fabien N, Field AC, Louedec L, Dai J, Joly E, Morelon E, Soulillou JP, Michel JB, Nicoletti A. Immune responses elicited in tertiary lymphoid tissues display distinctive features. PloS one. 2010; 5:e11398. [PubMed: 20613979]
29. Caspi, RR. Experimental autoimmune uveoretinitis in the rat and mouse. In: Coligan, John E., et al., editors. Current protocols in immunology. Vol. 15. 2003. p. 16
30. Karabekian Z, Lytton SD, Silver PB, Sergeev YV, Schneck JP, Caspi RR. Antigen/MHC class II/Ig dimers for study of uveitogenic T cells: IRBP p161–180 presented by both IA and IE molecules. Invest Ophthalmol Vis Sci. 2005; 46:3769–3776. [PubMed: 16186361]
31. Carson MJ, Reilly CR, Sutcliffe JG, Lo D. Mature microglia resemble immature antigen-presenting cells. Glia. 1998; 22:72–85. [PubMed: 9436789]
32. Chastain EM, Duncan DS, Rodgers JM, Miller SD. The role of antigen presenting cells in multiple sclerosis. Biochimica et biophysica acta. 2011; 1812:265–274. [PubMed: 20637861]
33. Wlodarczyk A, Lobner M, Cedile O, Owens T. Comparison of microglia and infiltrating CD11c(+) cells as antigen presenting cells for T cell proliferation and cytokine response. Journal of neuroinflammation. 2014; 11:57. [PubMed: 24666681]
34. Seifert M, Kuppers R. Molecular footprints of a germinal center derivation of human IgM+(IgD +)CD27+ B cells and the dynamics of memory B cell generation. The Journal of experimental medicine. 2009; 206:2659–2669. [PubMed: 19917772]
35. Leon B, Ballesteros-Tato A, Browning JL, Dunn R, Randall TD, Lund FE. Regulation of T(H)2 development by CXCR5+ dendritic cells and lymphotoxin-expressing B cells. Nat Immunol. 2012; 13:681–690. [PubMed: 22634865]
36. Guillemin GJ, Brew BJ. Microglia, macrophages, perivascular macrophages, and pericytes: a review of function and identification. Journal of leukocyte biology. 2004; 75:388–397. [PubMed: 14612429]
37. Rangel-Moreno J, Carragher DM, de la Luz Garcia-Hernandez M, Hwang JY, Kusser K, Hartson L, Kolls JK, Khader SA, Randall TD. The development of inducible bronchus-associated lymphoid tissue depends on IL-17. Nat Immunol. 2011; 12:639–646. [PubMed: 21666689]

38. Peters A, Pitcher LA, Sullivan JM, Mitsdoerffer M, Acton SE, Franz B, Wucherpfennig K, Turley S, Carroll MC, Sobel RA, Bettelli E, Kuchroo VK. Th17 cells induce ectopic lymphoid follicles in central nervous system tissue inflammation. Immunity. 2011; 35:986–996. [PubMed: 22177922]

39. Katakai T, Hara T, Sugai M, Gonda H, Shimizu A. Th1-biased tertiary lymphoid tissue supported by CXC chemokine ligand 13-producing stromal network in chronic lesions of autoimmune gastritis. J Immunol. 2003; 171:4359–4368. [PubMed: 14530361]

40. Chen J, Vistica BP, Takase H, Ham DI, Fariss RN, Wawrousek EF, Chan CC, DeMartino JA, Farber JM, Gery I. A unique pattern of up- and down-regulation of chemokine receptor CXCR3 on inflammation-inducing Th1 cells. European journal of immunology. 2004; 34:2885–2894. [PubMed: 15368305]

41. Prendergast RA, Iliff CE, Coskuncan NM, Caspi RR, Sartani G, Tarrant TK, Lutty GA, McLeod DS. T cell traffic and the inflammatory response in experimental autoimmune uveoretinitis. Invest Ophthalmol Vis Sci. 1998; 39:754–762. [PubMed: 9538882]

42. Thurau SR, Mempel TR, Flugel A, Diedrichs-Mohring M, Krombach F, Kawakami N, Wildner G. The fate of autoreactive, GFP+ T cells in rat models of uveitis analyzed by intravital fluorescence microscopy and FACS. Int Immunol. 2004; 16:1573–1582. [PubMed: 15351788]

43. Zhou R, Horai R, Silver PB, Mattapallil MJ, Zarate-Blades CR, Chong WP, Chen J, Rigden RC, Villasmil R, Caspi RR. The living eye “disarms” uncommitted autoreactive T cells by converting them to Foxp3(+) regulatory cells following local antigen recognition. Journal of immunology. 2012; 188:1742–1750.

44. McPherson SW, Heuss ND, Gregerson DS. Local “on-demand” generation and function of antigen-specific Foxp3+ regulatory T cells. Journal of immunology. 2013; 190:4971–4981.

45. Horai R, Zarate-Blades CR, Dillenburg-Pilla P, Chen J, Kielczewski JL, Silver PB, Jittayasothorn Y, Chan CC, Yamane H, Honda K, Caspi RR. Microbiota-Dependent Activation of an Autoreactive T Cell Receptor Provokes Autoimmunity in an Immunologically Privileged Site. Immunity. 2015; 43:343–353. [PubMed: 26287682]

46. Pennesi G, Mattapallil MJ, Sun SH, Avichezer D, Silver PB, Karabekian Z, David CS, Hargrave PA, McDowell JH, Smith WC, Wiggert B, Donoso LA, Chan CC, Caspi RR. A humanized model of experimental autoimmune uveitis in HLA class II transgenic mice. The Journal of clinical investigation. 2003; 111:1171–1180. [PubMed: 12697736]

47. Heiligenhaus A, Miserocchi E, Heinz C, Gerloni V, Kotaniemi K. Treatment of severe uveitis associated with juvenile idiopathic arthritis with anti-CD20 monoclonal antibody (rituximab). Rheumatology. 2011; 50:1390–1394. [PubMed: 21378109]

48. Jimenez-Alonso J, Omar M, Lopez-Nevot MA, Perez-Alvarez F, Toribio M, Hidalgo C, Sabio JM. CD5+ B cells and uveitis. Annals of the rheumatic diseases. 2002; 61:854–855. [PubMed: 12176820]

49. Wang RX, Yu CR, Dambuza IM, Mahdi RM, Dolinska MB, Sergeev YV, Wingfield PT, Kim SH, Egwuagu CE. Interleukin-35 induces regulatory B cells that suppress autoimmune disease. Nature medicine. 2014; 20:633–641.

50. Cockerham GC, Hidayat AA, Bijwaard KE, Sheng ZM. Re-evaluation of “reactive lymphoid hyperplasia of the uvea”: an immunohistochemical and molecular analysis of 10 cases. Ophthalmology. 2000; 107:151–158. [PubMed: 10647734]

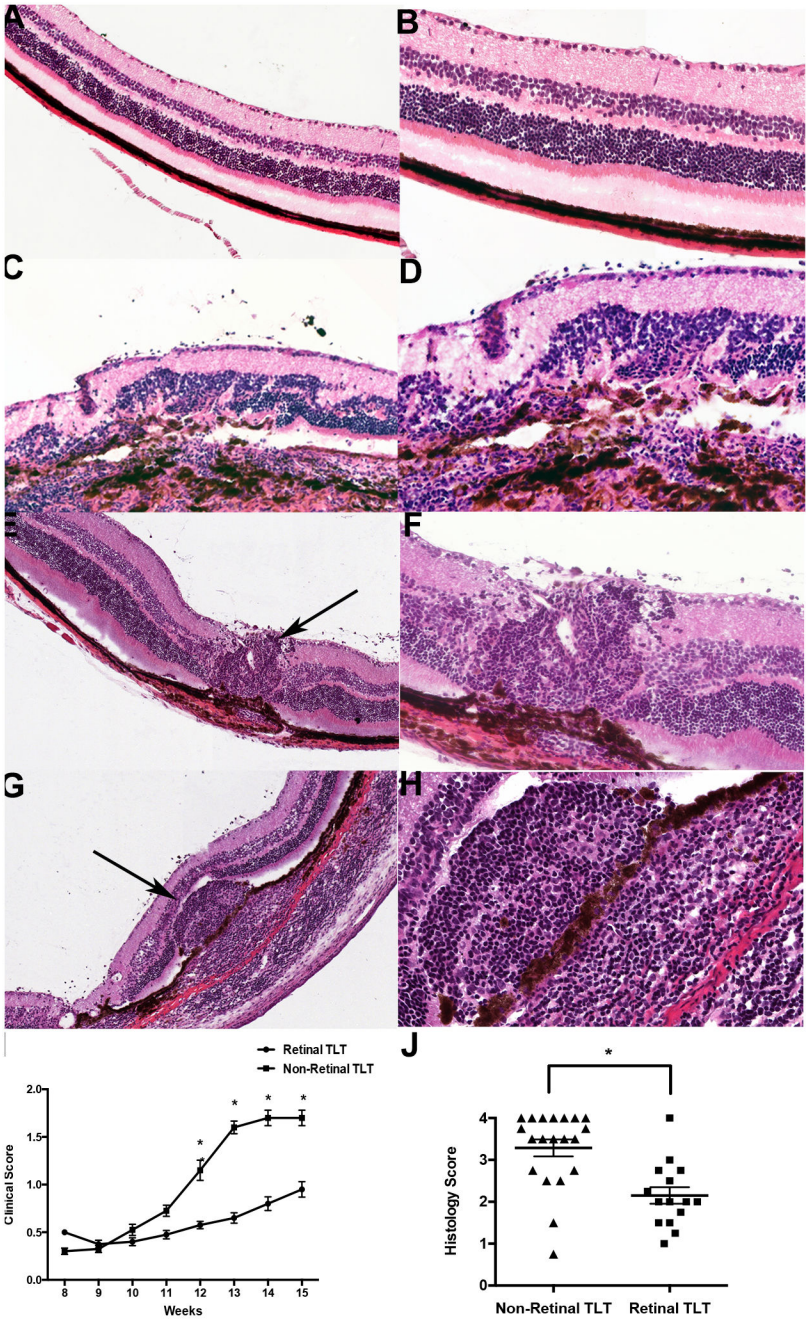

Figure 1. Representative H&E images of retinal lymphoid aggregates in R161H mice

A–B. Normal retina without lymphoid aggregates or inflammation under low magnification (20x) in **(A)** and under high magnification (40x) in **(B). C–D.** R161H retina without lymphoid aggregates at low magnification in **c** and under high magnification in **(D).** There is significant disruption of the retinal layers due to inflammation. **E, G.** Representative images of lymphoid aggregates in R161H retina under low magnification (20x). Black arrows denote a retinal lymphoid aggregate. **F&H.** High magnification (40x) images of the retinal aggregates shown under low magnification as shown in **(E, G)**. Note that the lymphoid aggregates vary in size and shape and are present in both the retina and choroid. **I.** Clinical

scores based on fundus examination over the course of 15 weeks between R161H mice with retinal tertiary lymphoid tissue (TLT) and without retinal TLT (n=10 mice per group). The mice with retinal lymphoid aggregates have a statistically significant lower clinical score (*$p<0.05$) compared to mice absent of these structures beginning at 12 weeks of age and even persists at 15 weeks of age. **J.** Histology scores of mice with retinal TLT aggregates and with non-retinal TLT aggregates between 8–16 weeks of age (n=20 mice per group). There is a statistically significant difference (*$p<0.007$) in disease score between the two groups based on retinal histology. P values were determined using paired Student's *t* test.

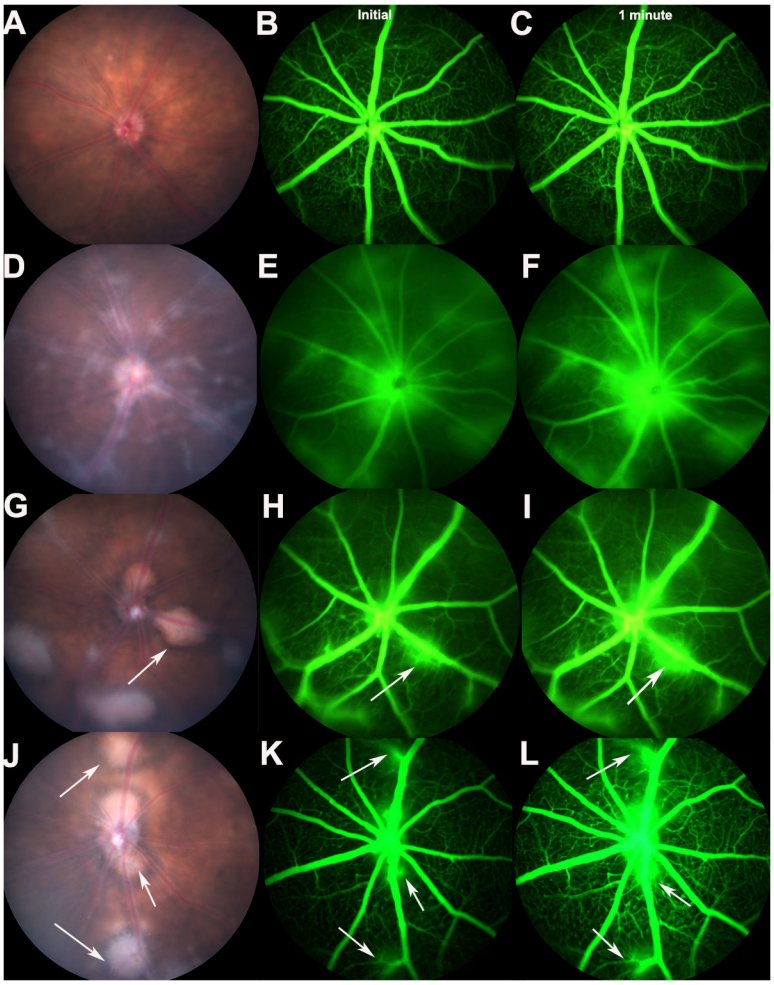

Figure 2. Fundus images showing retinal lymphoid aggregates in R161H mice and retinal vascular leakage around the lymphoid aggregates

A. Fundus of a normal mouse. **B, C.** Fluorescein angiography showing no retinal vascular leakage in a normal B10.RIII wild type mouse. **D.** Fundus of a R161H mouse without lymphoid aggregates. The fundus shows inflammation throughout the retina. **E&F.** Shows diffuse retinal vascular leakage throughout the retina. **G&J.** Fundus images of R161H mice with distinct retinal lymphoid aggregates. White arrows depict retinal lymphoid aggregates. **H, I, K, L.** Indicates vascular leakage surrounding the lymphoid aggregates. Angiography was repeated three times on three different mice from each group with consistent results. Initial images **(B, E, H, K**) were taken immediately after fluorescein injection and then 1 minute later **(C, F, I, L)** to show vascular leakage accumulation.

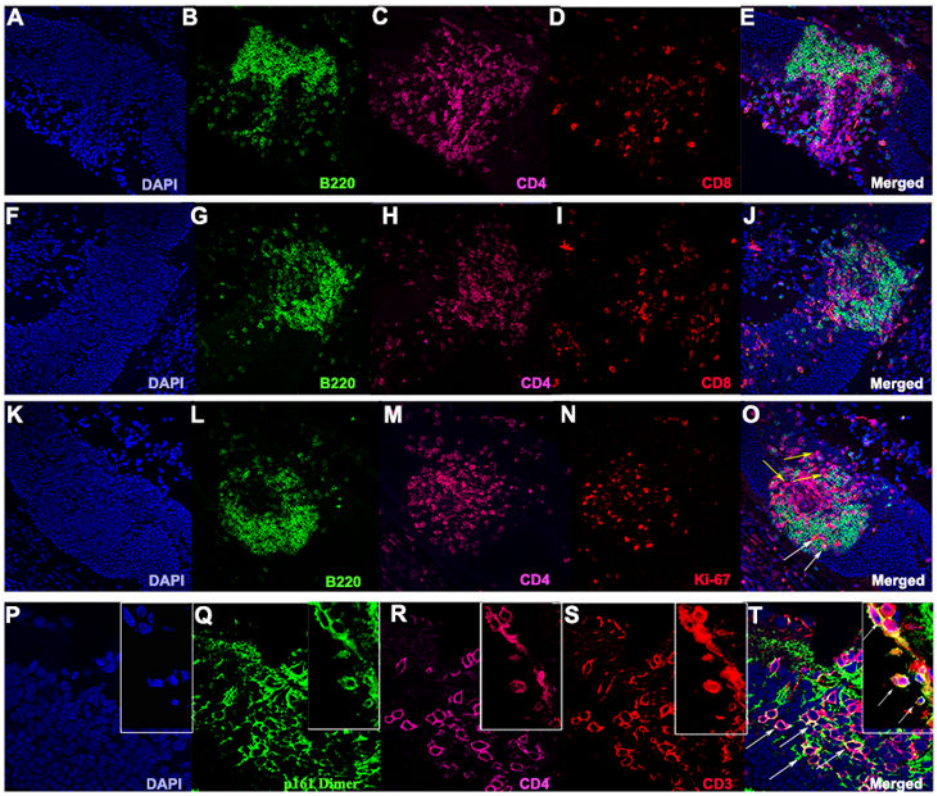

Figure 3. Retinal lymphoid aggregates are composed of proliferating B cells and CD4$^+$ T cells and contain IRBP-specific T cells

A–J. Examples of retinal lymphoid aggregates in two different R161H mice at high magnification (40x). **B, G.** Significant staining for the B cell marker B220 (green). **C, H.** Abundant CD4$^+$ T cell staining (magenta). **D, I.** Depicts a small population of CD8$^+$ T cells (red). **K–O.** Both B and T cells undergo cellular proliferation in the retinal aggregates as shown with Ki-67 (red) in (**N)** high magnification (40x). **O.** White arrows denote B220$^+$/Ki-67$^+$ B cells and yellow arrows show CD4$^+$/Ki-67$^+$ T cells. **P–T.** Shows the presence (white arrows) of R161TCR$^+$/CD4$^+$/CD3$^+$ cells expressing the T cell receptor specific for IRBP in the retinal lymphoid aggregates under high magnification (63x).

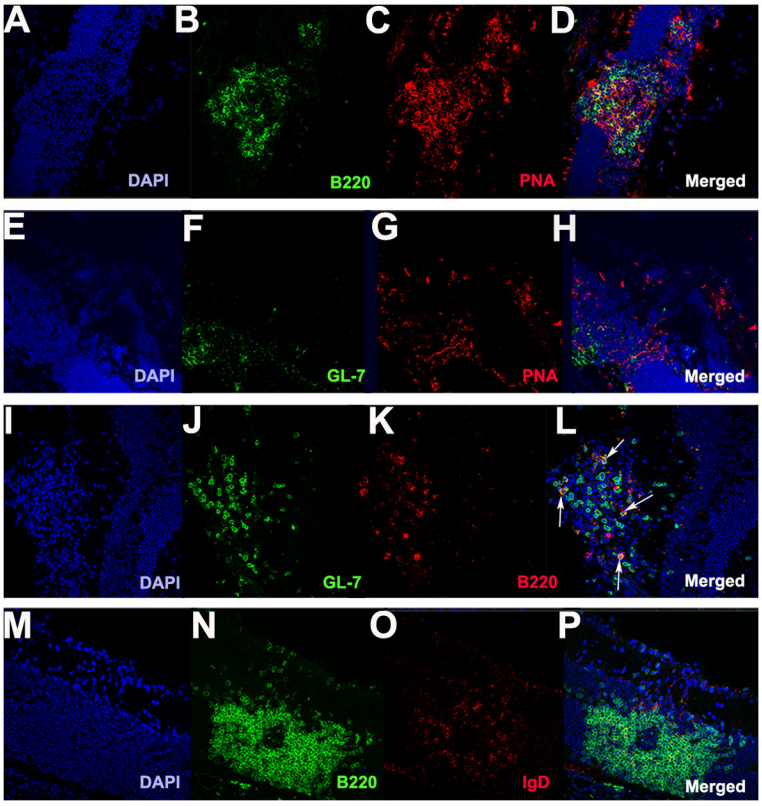

Figure 4. Retinal lymphoid aggregates stain positive for germinal markers PNA and GL-7 and low for IgD expression

A–P. Retinal lymphoid aggregates. **A–D.** Retinal lymphoid aggregates with a distinct B cell zone area (B220 shown in green) and staining positive for the germinal center marker PNA (red) as shown in **(C)** under low magnification (20x). **E–H.** Retinal aggregates stain positive for GL-7 (green) and PNA (red) under low magnification (20x). **I–L.** Depicts the presence of GL-7^+/$B220^+$ cells in the retinal aggregates under high magnification (40x). White arrows shown in L denote GL-7^+/$B220^+$ cells. **M–P.** Illustrates low IgD (red) expression in the retinal lymphoid aggregates under high magnification (40x).

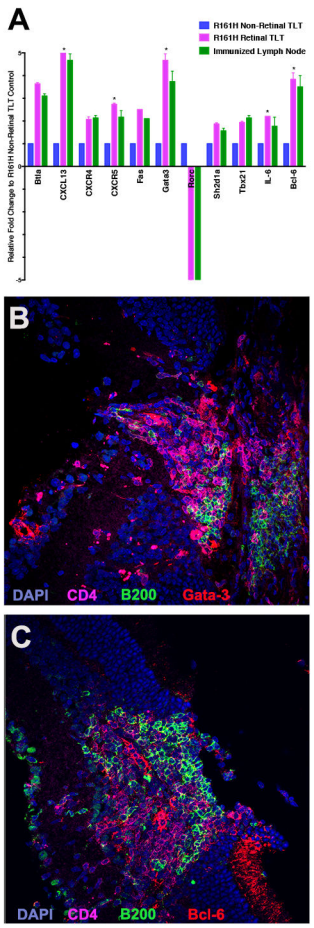

Figure 5. Retinal lymphoid aggregates have elevated expression of T-follicular helper genes by PCR analysis and immunohistochemical staining

A. Retinal lymphoid aggregates were isolated using laser capture microdissection (LCM). A total of five pooled R161H mice with distinct retinal TLT aggregates were analyzed and compared to R161H retina absent of retinal TLT aggregates. The positive control was true lymphoid follicles isolated from immunized lymph node from EAU mice. Gene arrays were repeated three times with consistent results. There was a statistically significant upregulation (*$p<0.05$) of CXCL13, CXCR5, Gata-3, IL-6 and Bcl-6 in the R161H retinal TLT compared to the R161H non-retinal TLT control retina. **B.** Immunohistochemical staining of retinal lymphoid aggregate for Gata-3 (red) B220 (green) CD4 T cell marker (magenta) and DAPI (blue) under high magnification (40x). **C.** Immunohistochemical staining of retinal lymphoid aggregate for Bcl-6 (red) B220 (green) CD4 T cell marker (magenta) and DAPI (blue) under high magnification (40x). P values were determined using Student's *t* test.

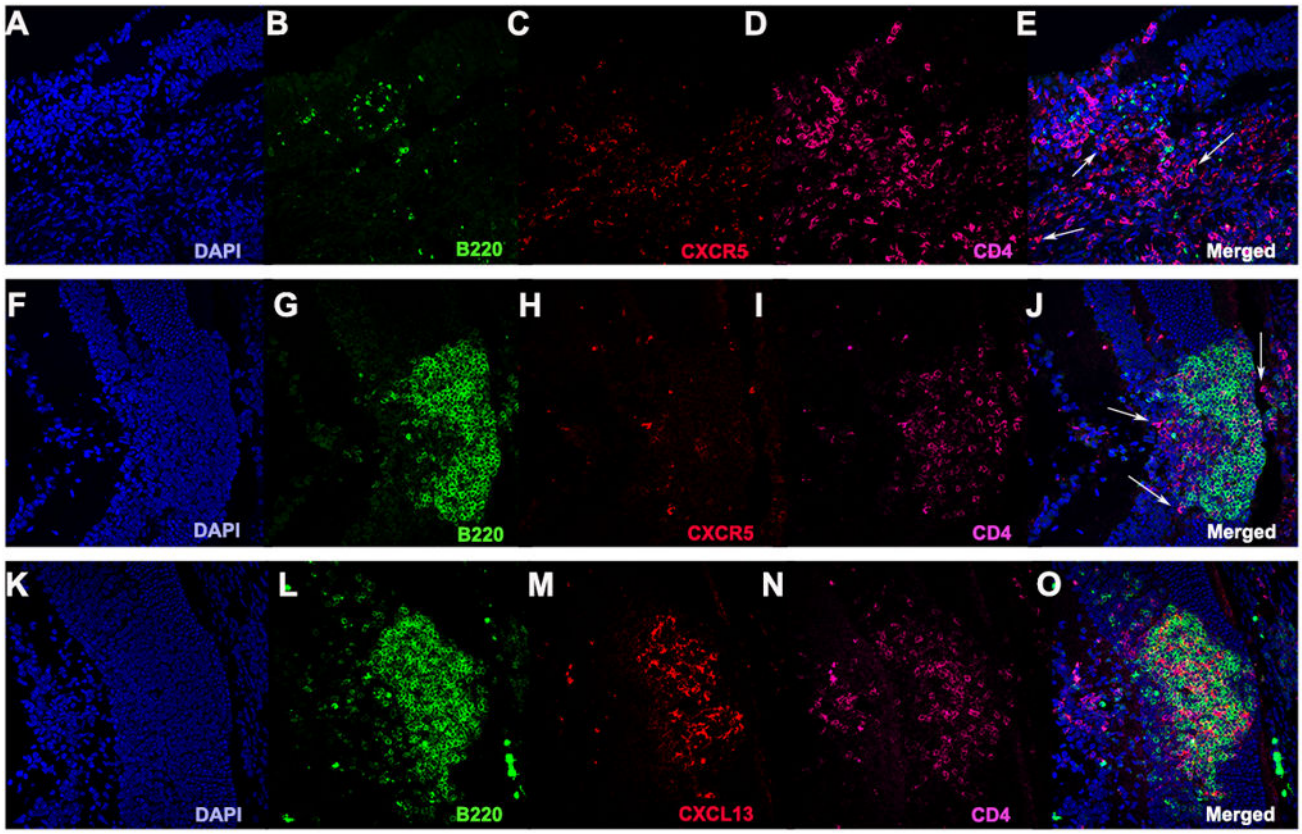

Figure 6. Retinal lymphoid aggregates contain CXCR5$^+$/CD4$^+$ T cells and highly express CXCL13, the ligand for CXCR5

A–J. Represents CXCR5$^+$/CD4$^+$ T cells are located in the retinal TLT under high magnification (40x). White arrows represent CXCR5$^+$/CD4$^+$ cells. **K–O.** Shows significant CXCL13 (red) expression in the retinal TLT.

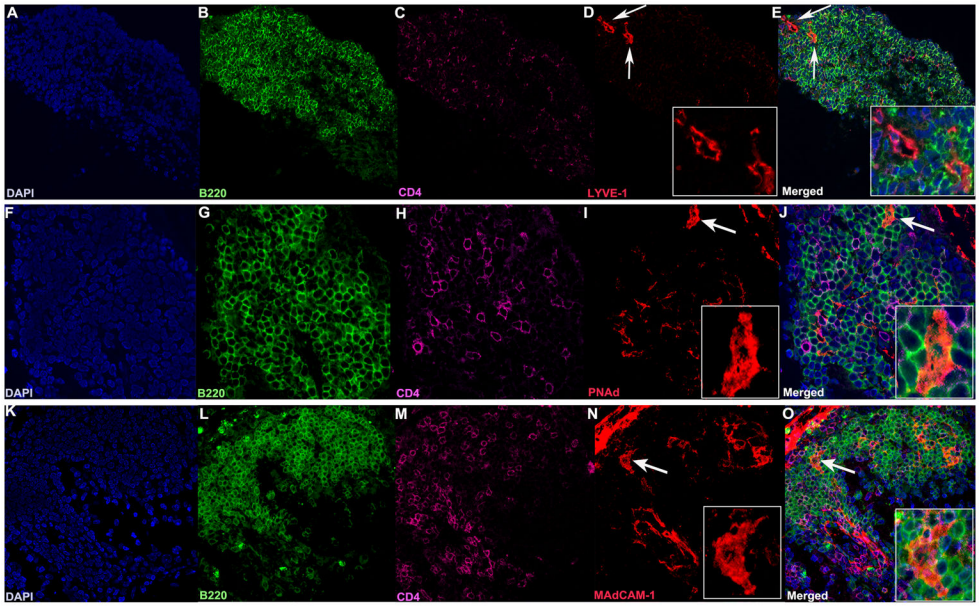

Figure 7. Lymphatic vessels and high endothelial venules are present in the retinal TLT

A–O. A–E. Lyve-1 staining (red) showing lymphatic vessels (white arrows 40x), enlarged in the inset (63x, panel D). **F–J**. PNAd staining (red), and **K–O** MAdCAM-1 staining (red) showing HEVs (white arrows, 40x), enlarged in the inset (63x panels I and N). Note their "plump" appearance, compared to panel D, typical of HEVs. Lymphocytes are present in and around the HEVs **(J, O).** Each marker was visualized on separate sections of the same TLT aggregate to avoid artifacts due to possible cross-reactivity between secondary antibodies.

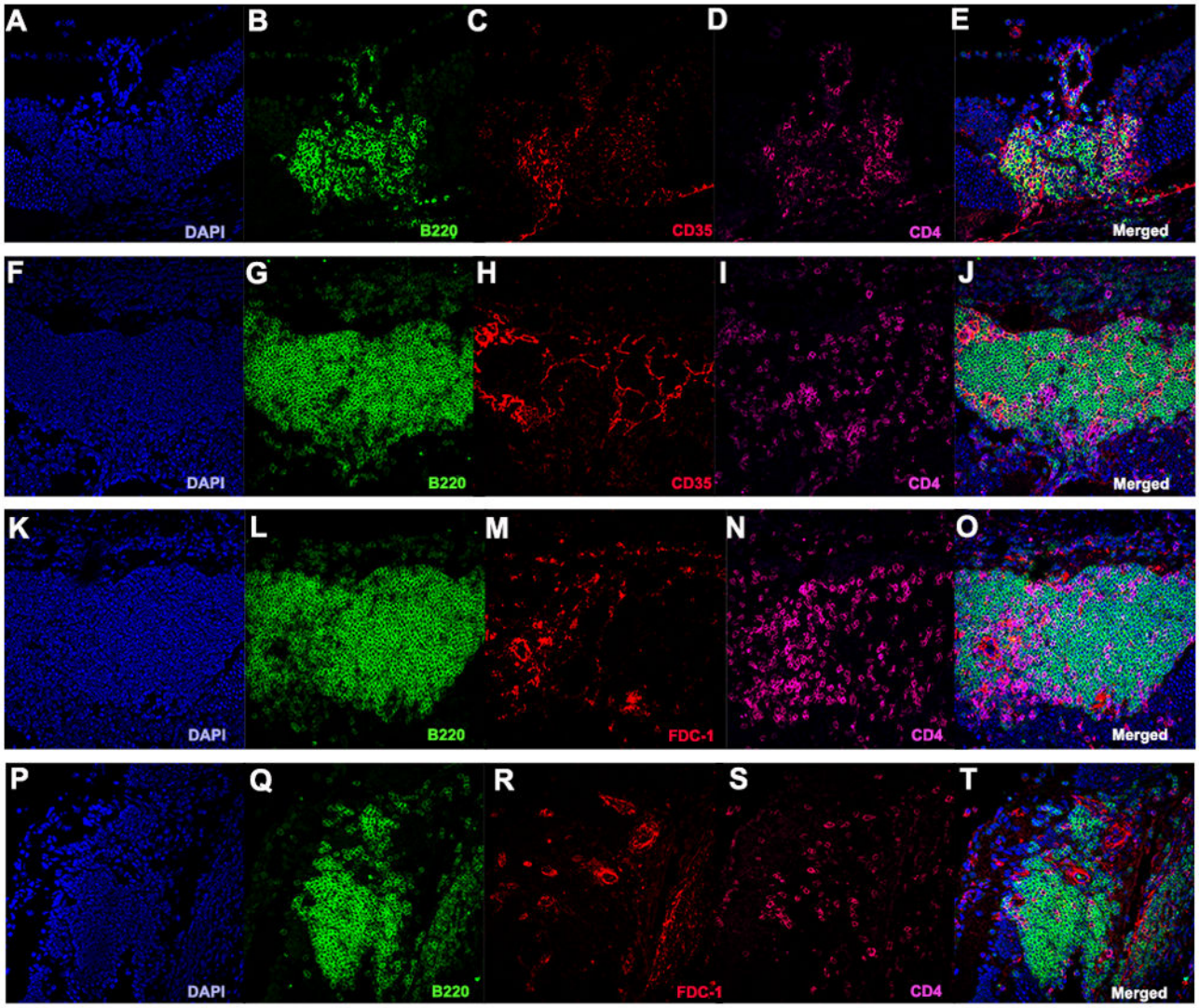

Figure 8. Retinal TLT stains positive for the stromal cell marker CD35 and follicular dendritic cell marker FDC-1, indicating the formation of organized networks within the retinal structures

A–J. Retinal TLT stained positive for CD35 (red). **K–T.** Retinal TLT stained for FDC-1 (red) under high magnification (40x).

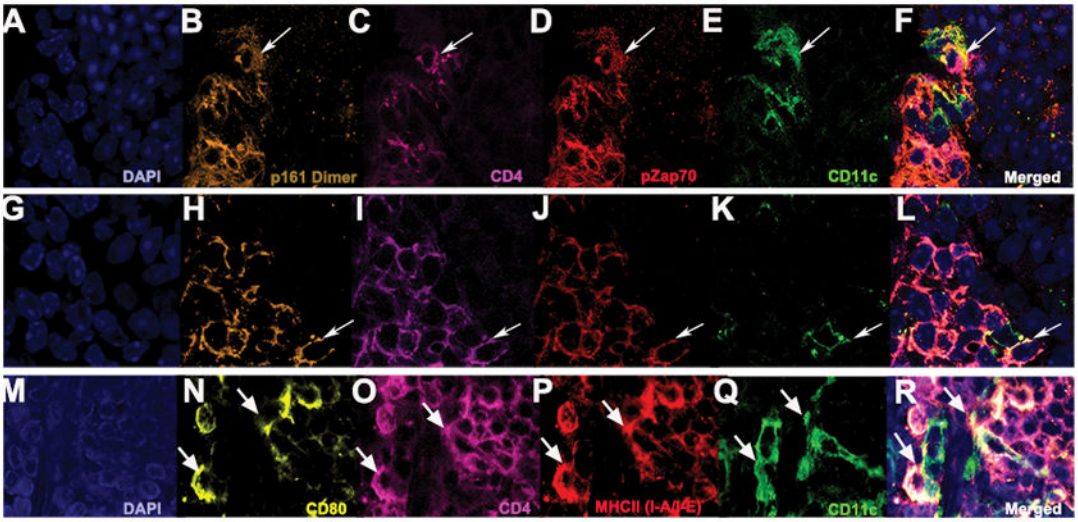

Figure 9. Presence of signaling through the IRBP specific T cell receptor in the immediate vicinity of CD11c$^+$ dendritic cells in the retinal TLT

A–L. White arrows denote co-localization between CD11c$^+$ dendritic cells (green) and CD4$^+$ T cells (magenta) specific for the T cell receptor for IRBP (gold) co-stained with pZap70 (red), suggesting that immune cell signaling occurs within the retinal TLT under high magnification (63x). **M–R.** Shows CD4$^+$ T cells (magenta) that are MHCII (I-A/I-E) positive (red) are closely associated with CD11c$^+$ cells (green) co-localized with CD80$^+$ (yellow), which is a co-stimulatory molecule needed for T cell activation under high magnification (63x).

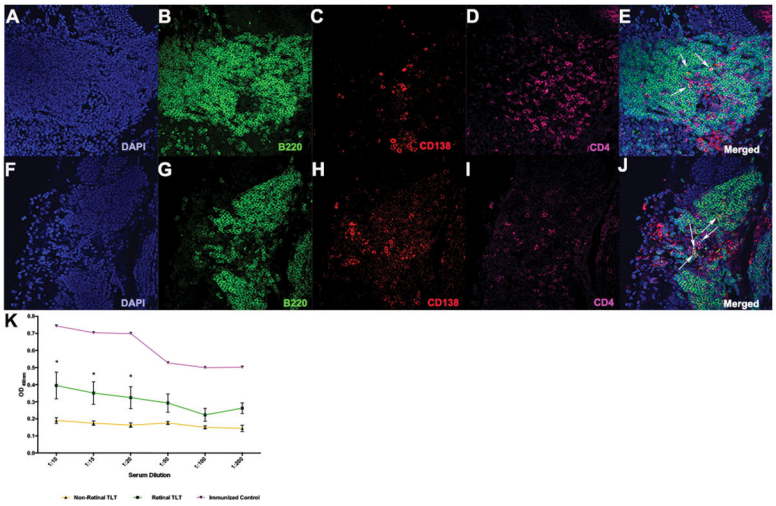

Figure 10. Retinal lymphoid aggregates contain CD138$^+$/B220$^+$ plasma cells and mice with retinal TLT have elevated serum antibodies to peptide 161-180 of the IRBP protein

A–J. CD138$^+$ cells (red) in well-defined retinal TLT under high magnification (40x). White arrows represent CD138$^+$/B220$^+$ cells under 40x magnification. **K.** ELISA analysis of serum auto-antibodies specific to the IRBP peptide 161-180 from R161H mice with and without retinal TLT structures. The positive control is wild-type B10.RIII mice immunized with the IRBP peptide 161-180. There is a significantly higher serum concentration of IRBP specific auto-antibodies in the mice with retinal TLT aggregates compared to mice without retinal TLT aggregates (*$p<0.05$). ELISA was repeated three times on five different mice from each group with consistent results. P values were determined using Student's *t* test.

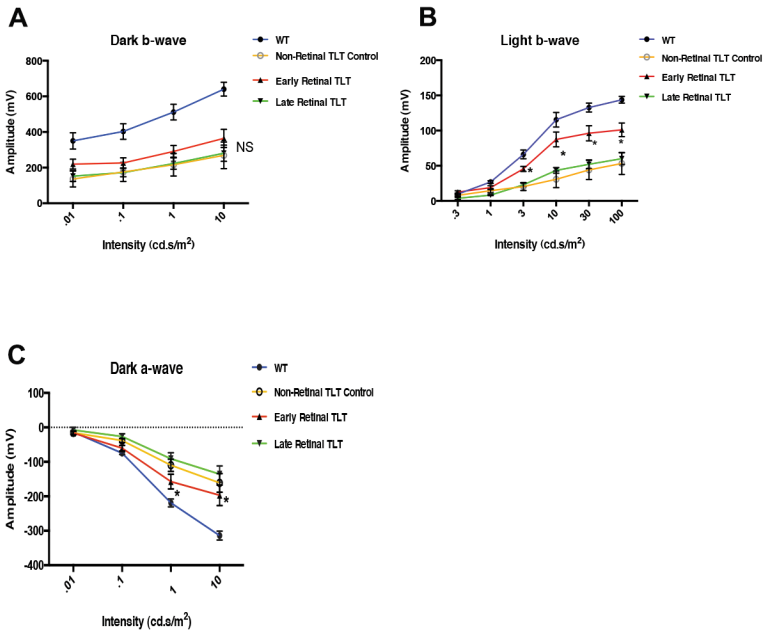

Figure 11. R161H Mice with early retinal TLT have a higher ERG response than R161H mice lacking TLT, but this advantage is lost in eyes with progressive late-stage TLT

R161H mice at 7–8 weeks of age and mice at 10–11 weeks of age were tested for visual function by ERG. **A.** There was no significant difference between R161H mice with early and late-stage retinal lymphoid aggregates for the dark b-wave ERG. **B.** There was a statistically significant higher light b-wave (*$p<0.05$) ERG response of R161H mice with early developing retinal TLT compared with the control R161H mice lacking retinal TLT structures or with late-stage retinal TLT. **C.** There was a statistically significant higher dark a-wave ERG response in R161H mice with early TLT aggregates (*$p<0.05$) compared to R161H mice lacking retinal TLT or with late-stage retinal TLT. ERG was repeated three times on at least five different mice from each group with reproducible results. P values were determined using one-way ANOVA.